Ubiquitin Binding Interface Mapping on Yeast Ubiquitin Hydrolase by NMR Chemical Shift Perturbation†

Sundaresan Rajesh,‡,§ Taiichi Sakamoto,||,⊥ Mariko Iwamoto-Sugai,|| Takehiko Shibata,‡ Toshiyuki Kohno,|| and Yutaka Ito*,‡

Laboratory of Cellular and Molecular Biology, Institute of Physical and Chemical Research (RIKEN), 2-1 Hirosawa, Wako, Saitama 351-0198, Japan, Department of Molecular Cellular Oncology and Microbiology, Faculty of Dentistry, Tokyo Medical and Dental University, 1-5-45 Yushima, Bunkyo, Tokyo 113-8549, Japan, and Mitsubishi Kasei Institute of Life Sciences, 11 Minamiooya, Machida, Tokyo 194-8511, Japan

Received February 18, 1999; Revised Manuscript Received May 6, 1999

ABSTRACT: The interaction between the 26 kDa yeast ubiquitin hydrolase (YUH1), involved in maintaining the monomeric ubiquitin pool in cells, and the 8.5 kDa yeast ubiquitin protein has been studied by heteronuclear multidimensional NMR spectroscopy. Chemical shift perturbation of backbone $^{1}H_N$, ^{15}N, and $^{13}C_\alpha$ resonances of YUH1, in a YUH1−ubiquitin mixture and in a 35 kDa covalent complex with ubiquitin (a stable analogue of the tetrahedral reaction intermediate), was employed to identify the ubiquitin binding interface of YUH1. This interface mapped on the secondary structure of YUH1 suggests a wide area of contact for ubiquitin, encompassing the N-terminus, α1, α4, β2, β3, and β6, coincident with the high specificity of YUH1 for ubiquitin. The presence of several hydrophobic clusters in the ubiquitin binding interface of YUH1 suggests that hydrophobic interactions are equally important as ionic interactions in contacting ubiquitin. The residues in the binding interface exhibit a high percentage of homology among the members of the ubiquitin C-terminal hydrolase family, indicating the well-conserved nature of the ubiquitin binding interface reported in this study. The secondary structure of YUH1, from our NMR studies, was similar to the recently determined structure of its human homologue ubiquitin C-terminal hydrolase L3 (UCH-L3), except for the absence of the helix H3 of UCH-L3. This region in YUH1 (helix H3 of UCH-L3) was least perturbed upon ubiquitin binding. Therefore, the binding interface was mapped onto the corresponding residues in the UCH-L3 crystal structure. A model for ubiquitin binding to YUH1 is proposed, in which a good correlation was observed for the lateral binding of ubiquitin to UCH-L3 (YUH1), stabilized by the electrostatic and hydrophobic interactions.

Ubiquitination is an obligatory step in the degradation of proteins by the ATP-dependent 26S−proteasome complex, a process that requires the covalent (isopeptide) linkage of the ubiquitin C-terminus with the lysine ϵ-amino groups of acceptor proteins (reviewed in refs *1*−*4*). The ubiquitin C-terminus can also be attached to α-amino groups via peptide bonds (*5*). Deubiquitinating enzymes release ubiquitin from the C-terminal extensions attached through either α-peptide or ϵ-amide linkages (reviewed in ref *6*). This serves to maintain the cellular pool of free ubiquitin and to regulate the overall rate of protein degradation. Deubiquitinating enzymes are broadly categorized into two distinct families of thiol proteases, ubiquitin-specific proteases (UBPs)[1] (*7*, *8*) and ubiquitin C-terminal hydrolases (UCHs) (*9*). There are at least 20 UBPs in yeast with molecular weight 50−300K that cleave large fusion proteins at the C-terminus of ubiquitin, exhibiting a broad range of substrate specificities and functions (*10*−*16*). The UCH enzymes (UCHs) are comparatively smaller (25−28 kDa) and preferentially cleave ubiquitin from ϵ-amide- and α-peptide-linked adducts and small peptides. UCHs prevent the depletion of the free ubiquitin pool by adduct formation with small nucleophiles (*9*). Other interesting functions include roles in neural development and differentiation of leukemia cell lines (*17*). Recently, an 82 kDa UCH activity was identified, BAP1, that functions as a tumor suppressor (*18*).

The *Saccharomyces cerevisiae (S. cerevisiae)* ubiquitin C-terminal hydrolase (YUH1) (*19*) has close homologues in mammals (UCH-L1, -L2, and -L3) (*20*) and *Drosophila melanogaster* (UBL-DROME) (*21*). Sequence alignment of the human UCH-L1 and -L3, YUH1, and UBL-DROME revealed only 17% identity in sequence (*22*), with an overall

† This work was supported in part by grants for the Biodesign and MR Sciences Research Programs from RIKEN to Y.I.

* To whom correspondence should be addressed. Fax: +81-48-467-5692. E-mail: ito@louise.riken.go.jp.

‡ Institute of Physical and Chemical Research (RIKEN).

§ Tokyo Medical and Dental University.

|| Mitsubishi Kasei Institute of Life Sciences.

⊥ Present address: Department of Industrial Chemistry, Chiba Institute of Technology, 2-17-1 Tsudanuma, Narashino, Chiba 275-0016, Japan.

[1] Abbreviations: 2D and 3D, two and three dimensional, respectively; CSI, chemical shift index; DTT, dithiothreitol; EDTA, ethylenediaminetetraacetic acid; HSQC, heteronuclear single-quantum correlation; IPTG, isopropyl β-D-thiogalactoside; NMR, nuclear magnetic resonance; NOE, nuclear Overhauser effect; NOESY, NOE spectroscopy; PAGE, polyacrylamide gel electrophoresis; Tris-HCl, tris(hydroxymethyl)-aminomethane hydrochloride; Ub, ubiquitin; UBPs, ubiquitin-specific proteases; UCH, ubquitin C-terminal hydrolase; UCH-L3, ubiquitin C-terminal hydrolase L3; YUH1, yeast ubiquitin hydrolase 1.

10.1021/bi9903953 CCC: $18.00
Published on Web 06/26/1999

similarity of 20%. On the contrary, YUH1 and UCH-L3 share a 30% identity and 60% homology. UCHs are specific for Gly at the P1 site, while ubiquitin peptide extensions with Pro at the P1′ site alone were nonhydrolyzable or very slowly hydrolyzable (*23*, *24*). [Amino acids N- and C-terminal to the scissile bond in the substrate are designated P1 and P1′, respectively, and the corresponding binding sites on the enzyme are S1 and S1′ (*25*).] In this aspect they are different from the papain family of thiol proteases which show broad P1 site specificity (*26*). Ubiquitin C-terminal peptide extensions of up to 72 residues can be cleaved by YUH1 while larger folded proteins are not cleaved (*19*, *23*). Interestingly, an ubiquitin−ubiquitin dimer could not be cleaved, though the presence of Met at the P1′ site does not hinder hydrolysis of other smaller peptide extensions (*19*, *23*). Similar results were obtained with mammalian UCHs as well (*24*). Null mutants of YUH1 are phenotypically normal, suggesting the presence of other UCHs or that UCHs and UBPs may have overlapping substrate specificities (*7*). Given the lack of specificity for the P1′ site by UCHs, it is possible that they recognize structural features in ubiquitin preferring a flexible C-terminus. Indeed, ubiquitin binds UCH-L3 with a submicromolar binding constant and ubiquitin aldehyde, mimicking the acyl-enzyme intermediate, is a tightly binding inhibitor (*22*, *27*).

Site-directed mutagenesis of UCH-L3 identified Cys90 (YUH1 numbering) as the active site nucleophile attacking the carbonyl carbon of Gly76 of ubiquitin, with His166 as the general base and Asp181 assisting in catalysis (*22*). Recently, the crystal structure of UCH-L3 was solved by X-ray crystallography and drew similarities with the papain family of cysteine proteases in employing a catalytic triad for hydrolysis (*28*). However, UCHs differ from other cysteine proteases in limiting nonspecific hydrolysis by being highly specific for the ubiquitin moiety of the substrate. Available experimental information, in the form of thermodynamic and biochemical data, failed to reveal the molecular basis of this specificity (*22*, *24*, *27*). A hypothetical model for ubiquitin binding based on the deduced structure of UCH-L3 proposed a disordered loop to be important in governing specificity toward ubiquitin (*28*). However, no structural information is available on the enzyme−ubiquitin complex that could reveal the role of specificity determinants and conformational changes accompanying ubiquitin binding in UCHs. Structural studies of the ubiquitin-bound enzyme by NMR spectroscopy are useful to address the above issues and to observe actual interactions between ubiquitin and UCHs. In this paper we describe the backbone resonance assignment and secondary structure of free YUH1 from triple-resonance NMR studies on bacterially expressed recombinant YUH1. Backbone resonance assignments were also obtained for a YUH1−ubiquitin mixture and a YUH1−ubiquitin covalent complex. The ubiquitin binding interface of YUH1, identified on the basis of chemical shift perturbation of YUH1 backbone $^{1}H_{N}$, ^{15}N, and $^{13}C_{\alpha}$ resonances, served to build a hypothetical model for the interaction of YUH1 (UCH-L3) with ubiquitin.

MATERIALS AND METHODS

Protein Expression. For YUH1 expression, *Escherichia coli* strain BL21 (DE3) (Novagen, Madison, WI) was transformed with the expression vector pET24a (Novagen, Madison, WI) containing the DNA for *S. cerevisiae* YUH1 (*29*). The uniformly ^{15}N-labeled YUH1 protein (^{15}N-YUH1) was obtained by growing bacteria at 37 °C in M9 minimal media (*30*), containing $^{15}NH_4Cl$ (Isotec, Miamisburg, OH) as the sole nitrogen source, supplemented with 3 mM $MgSO_4$, 0.1 mM $CaCl_2$, 150 mM thiamin, and 50 mg/L kanamycin. At an OD_{600nm} of ∼0.6, protein expression was induced by the addition of isopropyl β-D-thiogalactoside (IPTG) to a final concentration of 1 mM. After 6 h of further growth at 37 °C, cells were harvested, washed, and stored at −80 °C. Uniformly ^{15}N-labeled YUH1 with the combination of 50% random fractional deuteration (50% $^{2}H/^{15}N$-YUH1) was obtained in a similar manner by growing cells in M9 medium containing 60% $^{2}H_2O$/40% $^{1}H_2O$, with $^{15}NH_4Cl$ as the sole nitrogen source. Uniformly $^{13}C/^{15}N$-labeled YUH1 with the combination of 50% random fractional deuteration (50% $^{2}H/^{13}C/^{15}N$-YUH1) was obtained by growing cells in M9 medium containing 60% $^{2}H_2O$/40% $^{1}H_2O$, with $^{15}NH_4Cl$ and [^{13}C]-D-glucose as the sole nitrogen and carbon sources, respectively. Uniformly $^{13}C/^{15}N$-labeled YUH1 with the combination of ∼80% random fractional deuteration (80% $^{2}H/^{13}C/^{15}N$-YUH1) was obtained by growing cells in M9 medium containing 95% $^{2}H_2O$/5% $^{1}H_2O$. The deuteration efficiencies were confirmed by mass spectrometry.

For ubiquitin expression, *E. coli* BL21 (DE3) was transformed with the expression vector pET24a containing the DNA for *S. cerevisiae* ubiquitin (*29*). Unlabeled ubiquitin was obtained by growing the bacteria in LB broth (*30*) at 37 °C, initially to an OD_{600nm} of ∼0.6 unit. Expression was then induced by the addition of IPTG to a final concentration of 1 mM followed by growth for another 6 h. The cells were harvested, washed, and stored at −80 °C.

Protein Purification. All the procedures described below were carried out at 4 °C unless otherwise stated. For YUH1 purification the frozen cell pellets were thawed and resuspended to 0.1 g/mL with lysis buffer [50 mM Tris-HCl, pH 8.0, 2 mM DTT, 200 μg/mL Pefabloc (Boehringer-Manheim)]. Lysis was performed using lysozyme (0.1 mg/mL) for 30 min on ice followed by sonication to disrupt DNA. The cell debris was clarified by centrifugation at 10000*g* for 1 h. The supernatant was diluted 4-fold with buffer A (50 mM Tris-HCl, pH 8.0, 2 mM DTT), and proteins were purified by a succession of DEAE-Sepharose Fast Flow (Pharmacia) anion exchange, Sephadex G-75 Superfine (Pharmacia) gel filtration, and Q-Sepharose Fast Flow (Pharmacia) anion-exchange column chromatographic procedures. The YUH1 fractions were concentrated using Centriprep 10 concentrators (Amicon) and stored at 4 °C in storage buffer (50 mM Tris-HCl, pH 8.0, 10 mM DTT).

For ubiquitin purification, the cells were thawed and resuspended to 0.1 g/mL with lysis buffer (50 mM sodium acetate, pH 5.0, 2 mM DTT, 200 μg/mL Pefabloc). The cell suspension was sonicated vigorously and clarified by centrifugation at 10000*g* for 1 h. The clear supernatant was heated to 85 °C for 5 min, and denatured proteins were removed by centrifugation at 10000*g* for 1 h. The resulting supernatant containing ubiquitin was diluted 4-fold with buffer B (50 mM sodium acetate, pH 5.0, 2 mM DTT) and loaded onto an SP-Sepharose Fast Flow (Pharmacia) column preequilibrated with buffer B. The protein was eluted using a NaCl gradient and concentrated using a Centriprep 3

concentrator (Amicon). The protein was then loaded onto a Sephadex G-75 Superfine (Pharmacia) gel filtration column and eluted with buffer A. The ubiquitin fractions were concentrated and stored at −20 °C as lyophilized powder.

Preparation and Purification of the YUH1−Ubiquitin Covalent Complex. A covalent complex of 80% $^2H/^{13}C/^{15}N$-YUH1 with unlabeled ubiquitin was generated in a similar manner as reported earlier for a human UCH enzyme (*9*), with slight modifications. Briefly, a mixture of 1:5 molar equiv of 80% $^2H/^{13}C/^{15}N$-YUH1 and unlabeled ubiquitin, respectively, was treated with freshly prepared 2 mM $NaBH_4$ in a 50 mM Tris-HCl, pH 8.0, buffer containing 10 mM DTT at 37 °C for 60 min. Fresh $NaBH_4$ was added to the reaction mixture every 5 min due to its labile nature in aqueous solution. The reaction mixture was loaded onto a Q-Sepharose Fast Flow anion-exchange column, and the proteins were eluted with a 100−600 mM NaCl gradient in buffer A. The YUH1−ubiquitin covalent complex elutes at a much lower salt concentration than free YUH1 with a yield of about 80%. The purity of the complex was checked by native PAGE analysis.

Preparation of Protein Samples for NMR. Protein samples were concentrated and dissolved in NMR buffer (90% ^1H_2O/10% ^2H_2O containing 50 mM $Na_2HPO_4-NaH_2PO_4$, pH 6.0, 100 mM NaCl, 10 mM DTT) using Centricon 10 (for YUH1) or Centricon 3 (for ubiquitin) concentrators (Amicon). In the case of ubiquitin, lyophilized powder at the required molarity was resuspended with filtered Milli-Q water before being dissolved in NMR buffer. For the 80% random fractionally deuterated YUH1, the slowly exchanging deuterons were replaced with protons by treatment with 50 mM Tris-HCl, pH 9.0, 100 mM NaCl, 10 mM DTT buffer at 30 °C for 48 h. The high pH buffer was then exchanged with NMR buffer prior to measurement.

NMR Spectroscopy. All NMR experiments were recorded under identical conditions on 2−3 mM samples on Bruker DRX600 and ARX400 spectrometers. All spectra were processed on Silicon Graphics Indigo^2 and Indy computers with the Azara software package (W. Boucher, unpublished). For the 3D data, the two-dimensional maximum entropy method (2D MEM) (*31*) was applied to obtain resolution enhancement for the indirect dimensions. Briefly, the acquisition dimension of the triple-resonance 3D data was first processed by applying FFT with a cosine square window function, and the region containing amide proton resonances was extracted. Next, the remaining two indirect dimensions were processed with 2D MEM using the noise level parameter defined from the corresponding spectra processed by applying FFT for all three dimensions. All of the spectra were analyzed with the combination of customized macroprograms on the Ansig software (*32*, *33*).

Resonance Assignments for YUH1. All of the 3D triple-resonance experiments used for the assignments of YUH1 were performed on 50% $^2H/^{13}C/^{15}N$-YUH1 sample in NMR buffer. The backbone ^1H_N, $^{13}C_\alpha$, and ^{15}N, and side-chain $^{13}C_\beta$ resonance assignments were achieved by analyzing spin−spin connectivity on four types of 3D triple-resonance experiments, HNCA (*34*−*36*), HN(CO)CA (*37*, *38*), CBCANNH (*39*, *40*), and CBCA(CO)NNH (*35*, *40*), with deuterium decoupling (*41*). The 3D HNCA and HN(CO)CA spectra were acquired with a total of 64 (t_1, ^{13}C) × 22 (t_2, ^{15}N) × 512 (t_3, ^1H_N) complex points. The 3D CBCANNH and CBCA(CO)NNH spectra were acquired with a total of 32 (t_1, ^{13}C) × 22 (t_2, ^{15}N) × 512 (t_3, ^1H_N) complex points. The backbone $^1H_\alpha$ and $^{13}C'$ resonances were assigned by analyzing HCA(CO)NNH (*42*) and HNCO (*35*, *36*) spectra. The 3D HCA(CO)NNH spectrum was acquired with a total of 32 (t_1, ^1H) × 22 (t_2, ^{15}N) × 512 (t_3, ^1H_N) complex points, and the 3D HNCO spectrum was acquired with a total of 64 (t_1, ^{13}C) × 22 (t_2, ^{15}N) × 512 (t_3, ^1H_N) complex points.

Secondary Structure Analysis for YUH1. The secondary structure of YUH1 was determined by a combination of the chemical shift index method (*43*, *44*) and analysis of sequential, intermediate, and long-range NOEs (d_{NN} and $d_{\alpha N}$) from a 3D ^{15}N-separated NOESY−HSQC spectrum (*45*). This 3D NOESY spectrum was measured with a mixing time of 200 ms and a total of 100 (t_1, ^1H) × 22 (t_2, ^{15}N) × 512 (t_3, ^1H_N) complex points on 50% $^2H/^{15}N$-YUH1. This spectrum further aided the identification of slowly exchanging ^1H_N protons in YUH1.

Titration Experiments of YUH1 with Ubiquitin. ^{15}N-YUH1 was successively titrated with unlabeled ubiquitin in molar ratios of 1:0.25, 1:0.5, 1:1, 1:1.5, 1:2, and 1:3, respectively. The total volume was kept constant at 500 μL. 2D $^1H-^{15}N$ HSQC spectra were measured at each titration point in the above-mentioned order.

Backbone Resonance Assignments for YUH1 in the Presence of Ubiquitin. All 3D triple-resonance experiments used in the backbone assignments of ubiquitin-bound YUH1 were performed on (I) a mixture of 80% $^2H/^{13}C/^{15}N$-YUH1 and unlabeled ubiquitin in the molar ratio of 1:3 and (II) the covalent YUH1−ubiquitin complex of 80% $^2H/^{13}C/^{15}N$-YUH1 and unlabeled ubiquitin, with deuterium decoupling (*41*). The backbone ^1H_N, $^{13}C_\alpha$, and ^{15}N and side-chain $^{13}C_\beta$ resonance assignments were achieved by analyzing spin−spin connectivity on HNCA (*37*), HN(CO)CA (*39*), and HN(COCA)CB (*39*). The 3D HNCA and HN(CO)CA spectra were acquired with a total of 64 (t_1, ^{13}C) × 22 (t_2, ^{15}N) × 512 (t_3, ^1H_N) complex points. The 3D HN(COCA)CB spectrum was acquired with a total of 32 (t_1, ^{13}C) × 22 (t_2, ^{15}N) × 512 (t_3, ^1H_N) complex points.

RESULTS AND DISCUSSION

Backbone Resonance Assignment and Secondary Structure of YUH1. NMR studies of proteins over 200 amino acids have been made easier with the advent of deuteration. Complete deuteration of all but the exchangeable ^1H_N protons in such large proteins improves the sensitivity of some heteronuclear experiments (*36*, *38*, *41*, *46*). Complete deuteration was also shown to be useful for the observation of long-range NOEs between ^1H_N protons (*47*, *48*). It was recently reported that deuteration at a level of ∼50% optimized the sensitivity of experiments which are used to assign side-chain ^1H and ^{13}C resonances or to observe NOEs between carbon-attached and ^1H_N protons (*40*). Thus, a 50% deuterated sample was used for the resonance assignment of YUH1, the size of which is well within the current working limits of protein NMR. The backbone ^1H_N, $^{13}C_\alpha$, and ^{15}N and side-chain $^{13}C_\beta$ resonances of YUH1 were almost completely assigned by analyzing the triple-resonance 3D NMR experiments, HNCA, HN(CO)CA, CBCANNH, and CBCA(CO)NNH, performed on 50% $^2H/^{13}C/^{15}N$-YUH1. The 50% random deuteration successfully enhanced the sensitivity

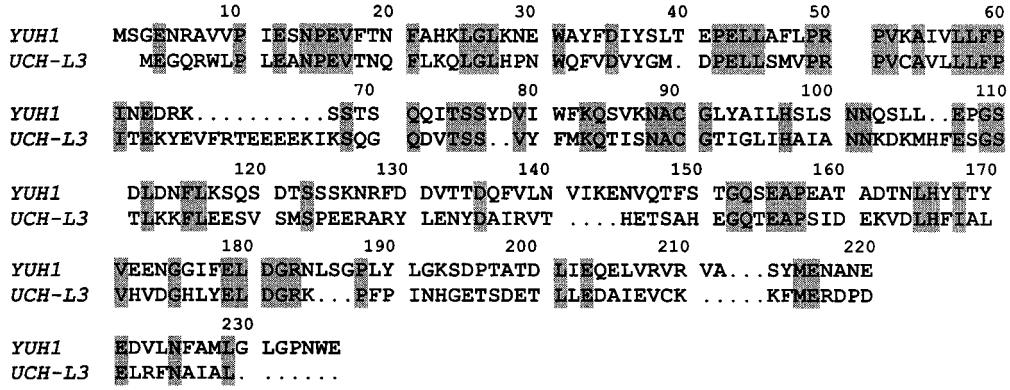

FIGURE 1: Sequence alignment of YUH1 and UCH-L3. Every tenth YUH1 residue, indicated in superscripts, is separated by a space. The identical residues are shown as shaded boxes. The sequence alignment was according to the Predict Protein Server algorithm (*52*).

of these triple-resonance experiments. We chose the combination of CBCANNH and CBCA(CO)NNH experiments over that of HNCACB and CBCA(CO)NNH for the present study. In fractionally deuterated proteins, protonated $^{13}C_\alpha$/C_β chemical shifts are obtained from CBCANNH and CBCA(CO)NNH experiments, while deuterated $^{13}C_\alpha/C_\beta$ will be mainly observed in the HNCACB experiment. Thus the latter combination gives rise to an isotope shift (~0.2 ppm) between HNCACB and CBCA(CO)NNH spectra, which could increase ambiguity during the assignment process. The backbone $^1H_\alpha$ and $^{13}C'$ resonances were assigned by analyzing HCA(CO)NNH and HNCO, respectively.

The secondary structure of YUH1, predicted on the basis of sequential, intermediate, and long-range NOE connectivities, and a consensus chemical shift index (CSI av) of $^{13}C_\alpha$, $^{13}C_\beta$, $^{13}C'$, and $^1H_\alpha$ shifts is summarized in Figure 2 (*43*−*45*). The identification of helices, based on sequential d_{NN} NOEs, intermediate-range NOEs, and a corresponding positive CSI av, revealed six helical regions in YUH1: helix α1 (16−23), a short helix α2 (43−46), long helices α3 (90−99), α4 (111−120), and α5 (132−144), and the C-terminal helix α6 (205−216). Helices α3 and α5 were identified predominantly on the basis of positive consensus CSI and intermediate-range NOEs. In addition to the above, slowly exchanging ^1H_N protons were found in the α-helical regions, indicating their protection due to hydrogen bonding.

In the case of YUH1, β-strands were identified from the following features: negative CSI av; strong and medium intensity sequential $d_{\alpha N}$ NOEs; long-range backbone−backbone NOEs; stretches of weak or missing sequential d_{NN} NOEs; and missing intermediate-range NOEs. Figure 3 shows the antiparallel contacts, defined by long-range backbone−backbone d_{NN} and $d_{\alpha N}$ NOEs assigned for residues between the following pairs of β-strands: β1 (30−36) and β6 (227−234); β6 and β2 (53−59); β2 and β3 (166−173); β3 and β4 (176−180); and finally β4 and β5 (189−191). The six antiparallel β-strands form a compact β-sheet structure possibly constituting the core of the protein. The emerging global fold of YUH1 (data not shown) also confirms this fact. The slowly exchanging ^1H_N protons further traced the above secondary structural elements. The complete secondary structure topology of YUH1 based on CSI and long- and medium-range NOE information, shown in Figure 4A, is comprised of six α-helical regions and a single β-sheet structure (constructed by the six antiparallel strands) connected by loop regions of varying lengths.

Comparison with the X-ray Structure of UCH-L3. With the backbone resonance assignments and predicted secondary structure of YUH1 in hand, we checked whether the high similarity in primary sequences between YUH1 and UCH-L3 (Figure 1) extends to the structural level as well by comparing their respective secondary structures. As expected, the secondary structure of YUH1 was almost identical to that of UCH-L3 (Figure 4). The β-sheet and most of the α-helical regions were conserved except for helix H3 of UCH-L3 (61−70 of YUH1). A negative CSI av and absence of sequential d_{NN} NOEs (Figure 2) in the above region argue against the presence of a helix in the NMR-derived secondary structure for YUH1. Instead, as seen in Figure 4A, only an extended loop structure seems to be feasible for this region. This can be explained in two ways. (I) Such a structural disparity might be due to the differences in amino acid sequence between UCH-L3 and YUH1 for this particular region. A comparison of sequences in this region (61−70), as in Figure 1, shows YUH1 to lack 10 residues from that of UCH-L3. Thus, this short region in YUH1 might disallow the formation of the helical structure seen in UCH-L3. (II) The helix H3 in the UCH-L3 crystal may be a consequence of the crystal packing effect. This region is exposed on the protein surface, and by generating neighboring molecules (through symmetric and parallel operation using the coordinates of the crystal structure), some intermolecular contacts could be seen.

In the UCH-L3 crystal structure (*28*), a loop region spanning residues 140−163 (YUH1 numbering) was disordered, possibly due to conformational polymorphism. Further, it was proposed that this structural multiplicity contributes to the ubiquitin binding specificity of UCH-L3 (*28*) and might be conserved among other UCH enzymes. To investigate this, we looked into our NMR results from YUH1 for this loop region. While the $^1H-^{15}N$ correlation cross-peaks in the 2D HSQC spectrum were strong and distinct for this region, very few intermediate/long-range NOEs were observed in the ^{15}N-separated NOESY−HSQC spectrum. This prompted us to speculate a highly flexible dynamic property for this loop region and offers an interesting coincidence with the UCH-L3 results. The role of this loop region in ubiquitin binding will be evident from the studies on Ub-bound YUH1, discussed below.

Binding Characteristics of YUH1 with Ubiquitin. UCHs generally hydrolyze short C-terminal extensions of ubiquitin with a lack of specificity for the leaving group that may vary

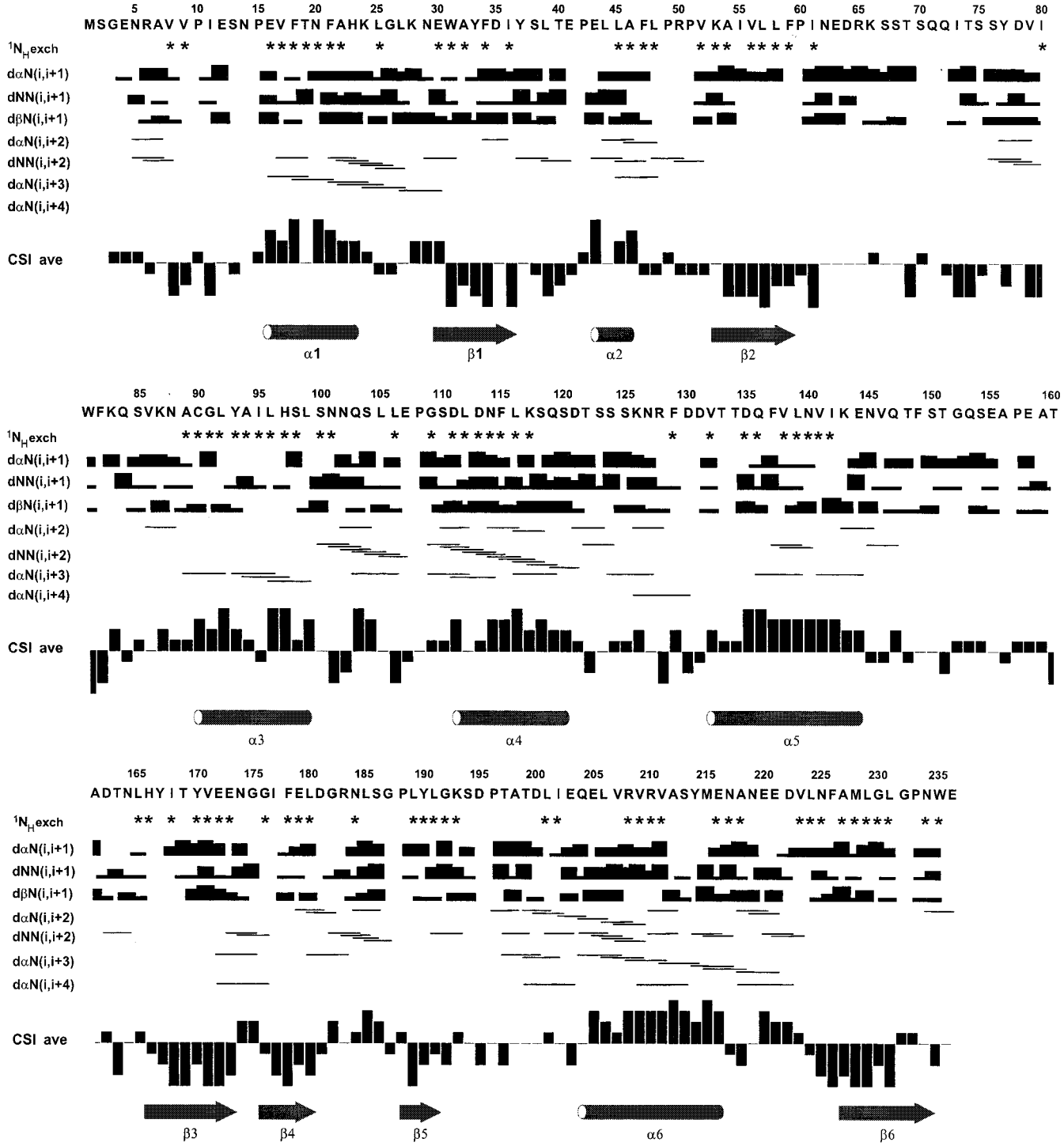

FIGURE 2: Summary of the observed ^1H_N exchange data, sequential and intermediate-range backbone NOEs, and consensus chemical shift index (CSI av), together with the derived secondary structure of YUH1. The consensus CSI av was calculated according to the equation CSI av = [(CSI $^{13}C_\alpha$ + CSI $^{13}C'$ − CSI $^{13}C_\beta$ − CSI $^1H_\alpha$)/4]. The height of each block in the sequential NOEs corresponds to the magnitude of the NOEs.

in size from simple $-NH_2$ groups to small proteins. They are, however, unable to cleave large or highly structured C-terminal extensions of ubiquitn, with certain exceptions (*24*). Thus, UCHs were proposed to recognize distinct structural features on the ubiquitin moiety of the fusions. This notion was also strengthened by the highly conserved 3D structure of ubiquitin across species (*49*, *50*). Indeed, ubiquitin, with a submicromolar binding constant, and ubiquitin aldehyde (a transition-state analogue inhibitor), with a picomolar binding constant, are tightly bound inhibitors of UCH enzymes (*22*, *27*). To identify the basis of this high specificity, we performed NMR studies on ubiquitin-bound YUH1.

A series of stepwise, multipoint titrations with ^{15}N-YUH1 and unlabeled ubiquitin were performed as described in Figure 5. 2D $^1H-^{15}N$ HSQC spectra were measured, first in the absence of ubiquitin and then at each titration point, to monitor YUH1 during formation of the complex. Ubiquitin addition affected YUH1 resonances in either of the following three ways: (I) no change in intensity and chemical shift or

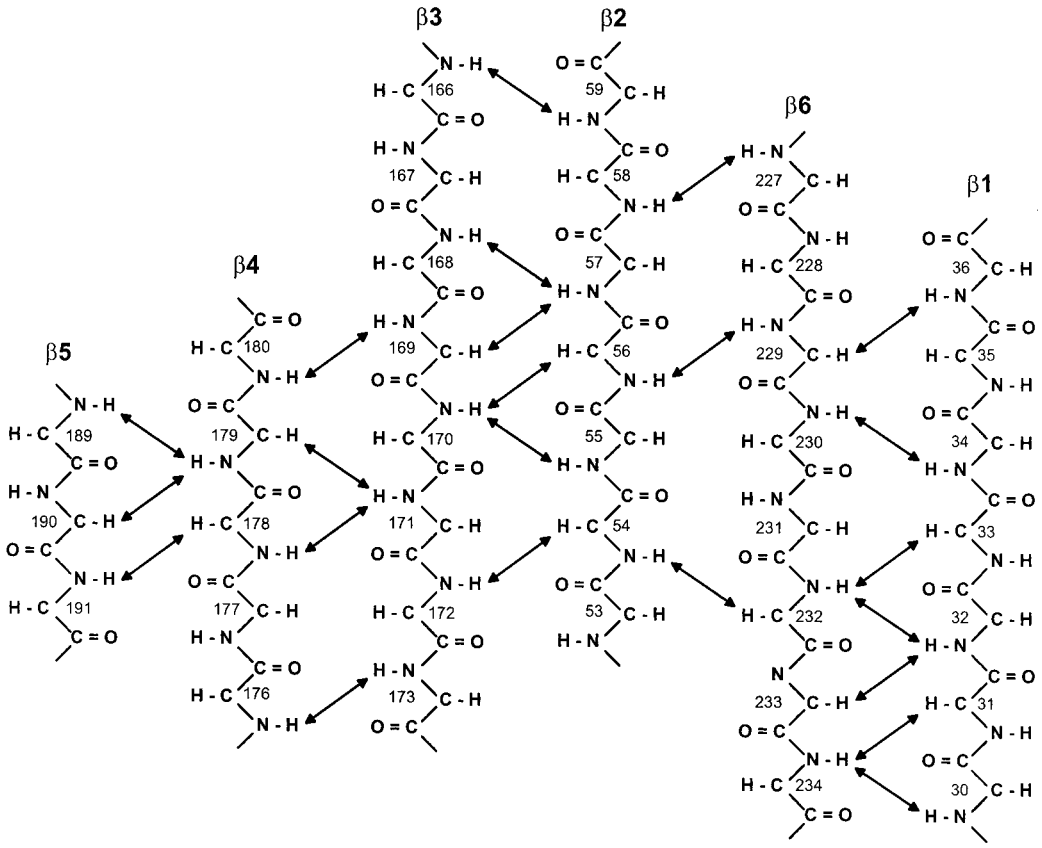

FIGURE 3: Topology diagram of the β-sheet structure in YUH1. Interstrand backbone NOEs are depicted as double-headed arrows.

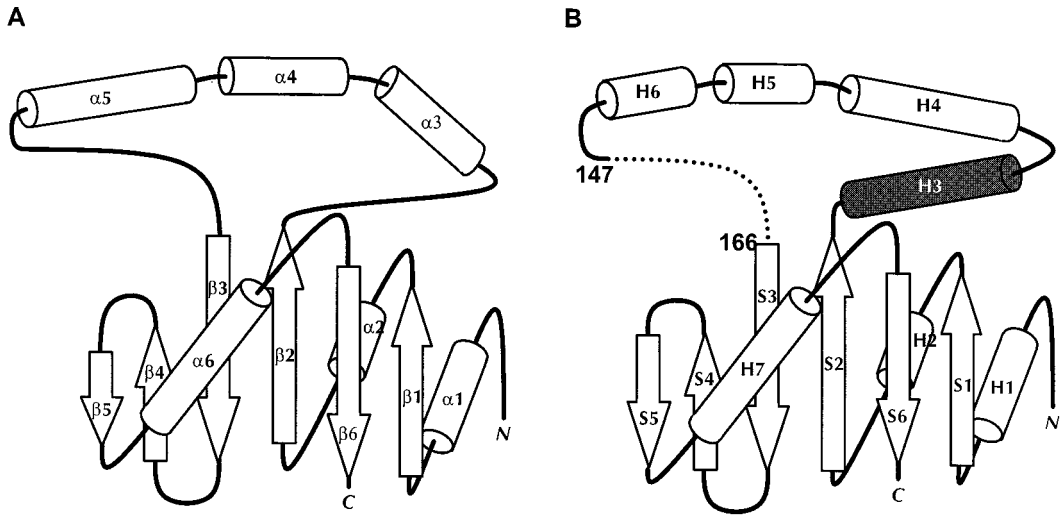

FIGURE 4: Secondary structure comparison of (A) YUH1 and (B) UCH-L3. The topology of UCH-L3 (*28*) was adapted to the emerging global fold of YUH1 for better understanding. The extra helix (H3) in UCH-L3 is shaded, and the disordered loop in UCH-L3 is indicated as a dotted line.

minor perturbation in chemical shift (e.g., residue S123 in Figure 5), (II) major perturbation of ^{1}H and/or ^{15}N chemical shift with intensity reduction (e.g., residue N145 in Figure 5), or (III) "missing" cross-peaks due to extreme line broadening (e.g., residue E41 in Figure 5). The large number of missing cross-peaks probably indicates an intermediate exchange situation between the free and ubiquitin-bound YUH1. This was further confirmed by increasing the ubiquitin concentration stepwise to a 3-fold molar excess over YUH1. This exercise failed to result in the emergence of a distinct set of cross-peaks, a general indicator of slow exchange. The line-broadened signals might be the direct result of the large difference in chemical shifts between the two states. Thus, the characterization of line-broadened signals in this intermediate exchange situation would probably highlight the ubiquitin binding interface on YUH1. Simple tracing and chemical shift assignment of ^{1}H−^{15}N correlation cross-peaks in ubiquitin-bound YUH1 were hampered by the exchange broadening and the spectral overlap. Hence, we performed triple-resonance experiments, initially on a 1:3 molar mixture of 80% ^{2}H/^{13}C/^{15}N-YUH1 and unlabeled ubiquitin (henceforth referred to as the YUH1−Ub mixture), respectively, to obtain unambiguous assignment.

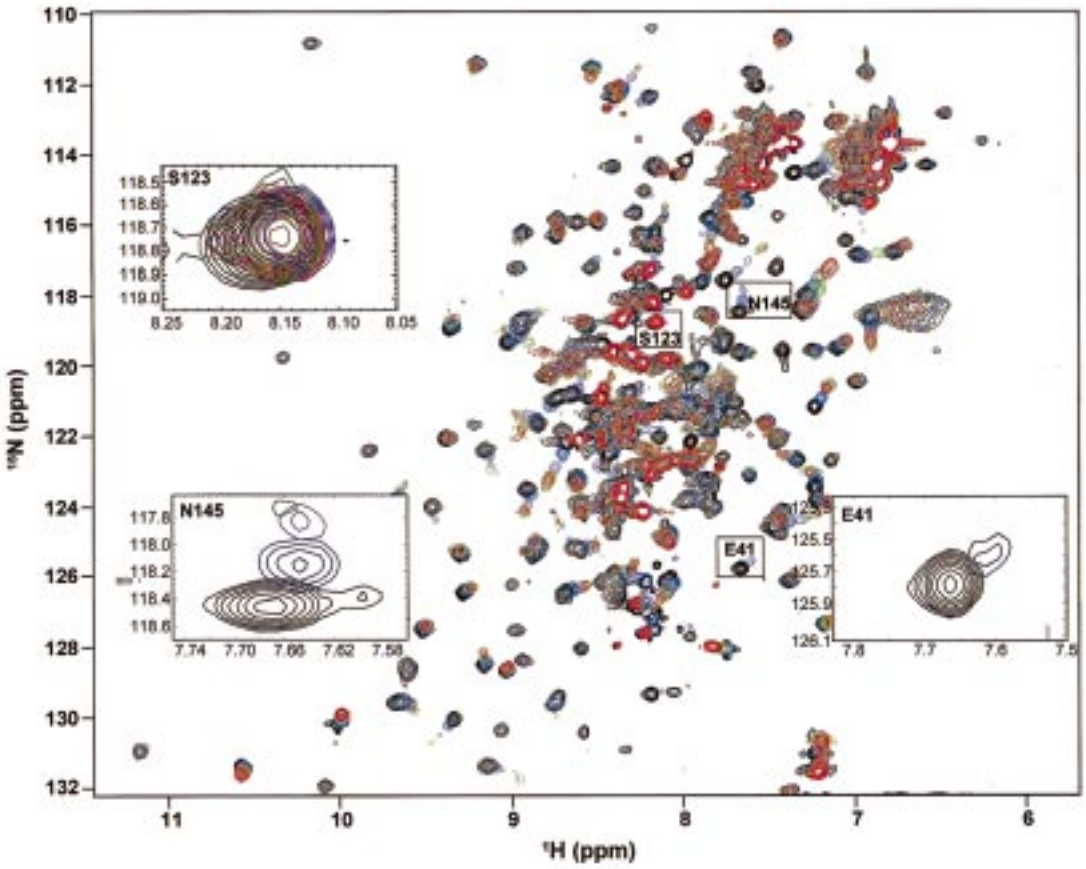

FIGURE 5: Overlays of 2D ^{1}H−^{15}N HSQC spectra from multipoint titrations of ^{15}N-YUH1 with unlabeled ubiquitin. The color codes of ^{1}H−^{15}N correlation cross-peaks at each titration point, showing the molar ratio of YUH1−Ub, are as follows: black (1:0); blue (1:0.25); purple (1:0.5); green (1:1); red (1:2). Shown as insets are representative cross-peaks for the intermediate exchange between free and ubiquitin-bound YUH1: (S123) no change in shift or intensity; (N145) cross-peak shift with intensity reduction; (E41) severely line-broadened.

Backbone Resonance Assignment of YUH1 in the YUH1−Ubiquitin Mixture. The ubiquitin-bound YUH1 has an approximate size of 35 kDa, which is around the maximum for protein NMR. Hence, an 80% deuterated YUH1 sample was chosen over that of a 50% deuterated one to optimize the sensitivity of heteronuclear triple-resonance experiments in the backbone assignment. 3D NMR experiments HNCA, HN(CO)CA, and HN(COCA)CB were performed on the YUH1−Ub mixture to assign $^{1}H_N$, ^{15}N, $^{13}C_\alpha$, and $^{13}C_\beta$ resonances. Complete backbone resonance assignment was possible for 68% of the residues. For residues lacking $^{13}C_\alpha$ correlation in the HNCA spectrum (A7, T40, T19, A54, Q71, F82, Q83, T163) but observed in the ^{1}H−^{15}N HSQC spectrum with negligible perturbation, tentative assignment of ^{1}H and ^{15}N was achieved by tracing the chemical shift values from free YUH1. Signal overlap in the ^{1}H−^{15}N dimension prevented the assignment for residues W31, N140, K143, V146, F149, and S150. We were unable to assign backbone resonances for the remaining (27%) non-proline residues due to line broadening in the ^{1}H, ^{15}N, and ^{13}C dimensions, consistent with the titration experiments. The residues with severe line broadening are discussed further in the following paragraph.

Chemical Shift Perturbation in the YUH1−Ub Mixture. As mentioned earlier, line broadening of NMR resonances is a common phenomenon at the regions involved in intermolecular contact, when the interaction is on an intermediate time scale. In addition to this, chemical shift perturbation of backbone resonances is also widely employed to determine the interaction surface, since the presence of an interacting group in close proximity tends to affect the chemical environment of residues in the interface. Thus, the elucidation of line-broadened and chemical shift perturbed residues is important in defining the ubiquitin binding interface of YUH1 in our system.

For all the backbone assigned residues in the YUH1−Ub mixture, the mean difference in ^{1}H, ^{15}N, and $^{13}C_\alpha$ chemical shifts, Δ_{av}, from their corresponding values in free YUH1 was calculated. For the sake of ensuing discussions, the residues are arbitrarily classified on the basis of their degree of chemical shift perturbation into unperturbed ($\Delta_{av} < 100$ Hz), least perturbed (100 Hz $\leq \Delta_{av} <$ 200 Hz), moderately perturbed (200 Hz $\leq \Delta_{av} <$ 500 Hz), and severely perturbed ($\Delta_{av} \geq$ 500 Hz) and color-coded as described in Figure 6 (^{1}H frequency was 600 MHz). In addition, the residues in which ^{1}H−^{15}N correlation cross-peaks were extremely broadened are shown in red. The Ub-induced chemical shift perturbation of YUH1 backbone atoms, together with the information from broadened residues, was mapped on the secondary structure of YUH1 (Figure 6A). The majority of line-broadened residues were located over a wide area on the surface of YUH1: around the N-terminal loop, α1, β2, loop L4, α3, loop L6, α5, β3, β4, and β6. Residue I142 displayed the maximum Δ_{av} of 779 Hz, while residues 20, 21, 27, and 38 showed moderate perturbation (200 Hz $\leq \Delta_{av} <$ 500 Hz). The remaining residues (~64% of non-proline residues) were unperturbed ($\Delta_{av} <$ 100 Hz) or least perturbed (100 Hz $\leq \Delta_{av} <$ 200 Hz) by ubiquitin binding.

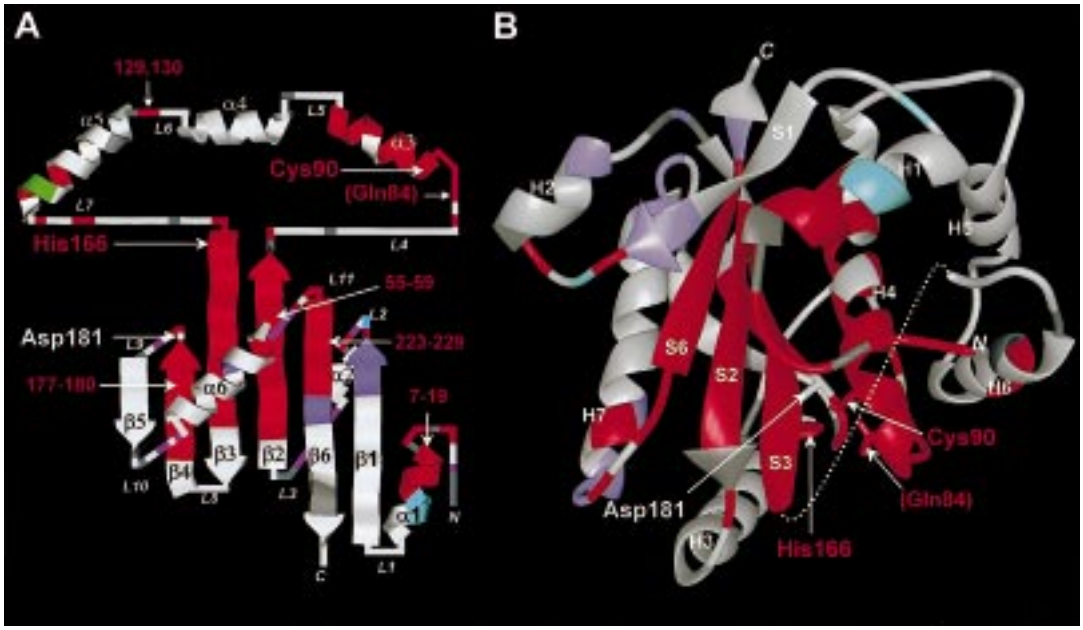

FIGURE 6: Chemical shift perturbation of backbone $^{1}H_N$, ^{15}N, and $^{13}C_\alpha$ nuclei in the YUH1−Ub mixture. (A) YUH1 residues affected by ubiquitin binding mapped onto the secondary structure of YUH1. (B) YUH1 residues affected by ubiquitin binding mapped onto the UCH-L3 crystal structure (*28*). The disordered loop in the crystal structure is shown as a dotted line. In the case of (B) UCH-L3 numbering was converted to that of YUH1 as in Figure 1. The backbone resonance affected residues upon ubiquitin binding are displayed color-coded. The mean shift difference, Δ_{av}, for each amino acid was calculated as $[(\Delta^1H_N)^2 + (\Delta^{15}N)^2 + (\Delta^{13}C_\alpha)^2]^{1/2}$, where Δ^1H_N, $\Delta^{15}N$, and $\Delta^{13}C_\alpha$ are the chemical shift differences (Hz) between free YUH1 and the YUH1−Ub mixture for resonances $^{1}H_N$, ^{15}N, and $^{13}C_\alpha$ observed at 14.1 T (^{1}H frequency is 600 MHz), respectively. The color coding is as follows: white ($\Delta_{av} \leq 100$ Hz); purple (100 Hz $\leq \Delta_{av} <$ 200 Hz); cyan (200 Hz $\leq \Delta_{av} <$ 500 Hz); green (500 Hz $\leq \Delta_{av} <$ 1000 Hz); yellow (1000 Hz $\geq \Delta_{av}$). The residues that were exchange broadened upon ubiquitin binding are shown in red. Proline and residues lacking chemical shift difference information are colored gray. The active site residues (YUH1 numbering) are indicated, and their side chains are highlighted.

Results from this mapping suggest that ubiquitin binds to a distinct and wide surface on YUH1, as evident from the large number of exchange-broadened residues. The binding interface, based on line-broadened regions, includes residues that are vicinal to the putative catalytic center and also several invariant hydrophobic and acidic residues. The extensive perturbation of backbone resonances reveals that the interaction is not restricted to side-chain-mediated events but also involves substantial conformational changes around the binding surface of YUH1.

Due to the availability of a high-resolution 3D crystal structure of the human homologue of YUH1, UCH-L3, we mapped the chemical shift changes onto the X-ray structure (*28*), as shown in Figure 6B. A 60% homology and 30% identity at the amino acid level, and considerable similarity in the secondary structure between YUH1 and UCH-L3 (Figure 4), encouraged such an approach. Moreover, the loop L4 of YUH1, corresponding to helix H3 of UCH-L3 (the only region structurally different between the two proteins), was least perturbed by ubiquitin interaction. As evident from Figure 6B, an excellent correlation could be observed for the interaction of YUH1 with ubiquitin, favoring a lateral binding mediated by residues in strands S2, S3, and S6 and helices H1 and H4 (colored red). Thus our results with the YUH1−Ub mixture define a broad area of protein−protein contact between YUH1 and ubiquitin.

However, the large number of exchange-broadened residues failed to reveal the extent of perturbation around these regions. To address this, we need to have a tight binding of ubiquitin to YUH1 or an ubiquitin-conjugated nonhydrolyzable inhibitor of YUH1. Toward this effect, we prepared a stable covalent complex of ubiquitin-bound YUH1 by arresting ubiquitin at the active site of YUH1 (*9*) and employed an experimental strategy similar to that for the YUH1−Ub mixture.

Backbone Resonance Assignment of YUH1 in a YUH1−Ubiquitin Covalent Complex. UCH enzymes hydrolyze their substrates through a conserved mechanism that involves the nucleophilic attack on the carbonyl carbon of G76 of ubiquitin by the thiol moiety of the active site cysteine residue (*9*). The acyl-enzyme intermediate, Ub(Gly)-C(O)-SH-(Cys)E, formed is then hydrolyzed to liberate free enzyme and ubiquitin (*9*). This acyl-enzyme intermediate can be trapped by borohydride to give a very stable hemithioacetal [Ub(Gly)-C(OH)S-(Cys)E], analogous to the true tetrahedral reaction intermediate (*9*). For the present study, we purified this hemithioacetal and utilized it to identify the ubiquitin binding sites in YUH1. This 35 kDa covalent complex between 80% $^{2}H/^{13}C/^{15}N$-YUH1 and unlabeled ubiquitin (henceforth referred to as the YUH1−Ub complex) was fairly stable under the NMR conditions used in this study (no major change in the $^{1}H-^{15}N$ HSQC spectrum after the 3D experiments; data not shown). The $^{1}H-^{15}N$ HSQC spectrum of this sample revealed the presence of many new cross-peaks previously absent in the YUH1−Ub mixture (Figure 7). Sequence-specific assignment of backbone resonances for YUH1 in the YUH1−Ub complex was done in a manner similar to that for the YUH1−Ub mixture. Backbone resonance assignment was possible for 90% of non-proline residues. For the remaining residues, lack of sequential connectivities, due to low intensity in HNCA, HN(CO)CA, and HN(COCA)CB, prevented the unambiguous assignment of backbone resonances. For example, residues V9, I55−F59, N88, F129−D131, E158−T160, and N164−T169 were

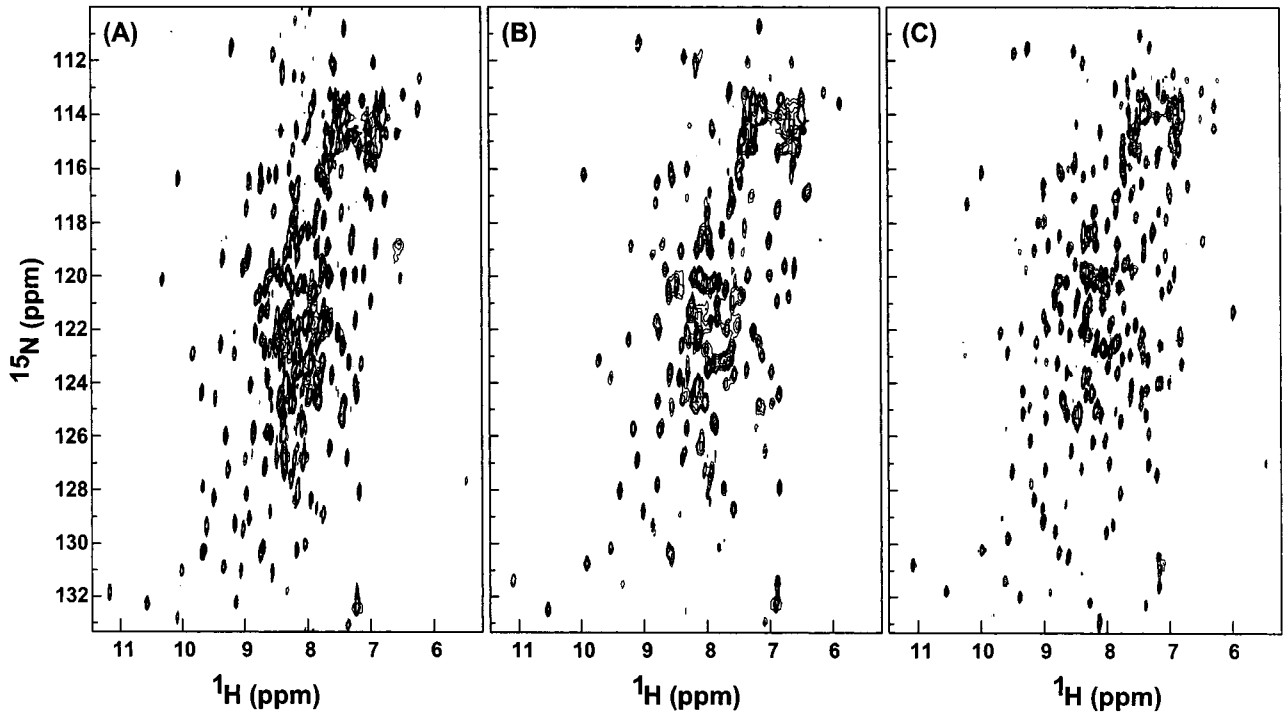

FIGURE 7: Comparison of the contour plots of ^{1}H−^{15}N HSQC spectra of (A) 50% ^{2}H/^{13}C/^{15}N-YUH1, (B) the YUH1−Ub mixture, and (C) the YUH1−Ub covalent complex.

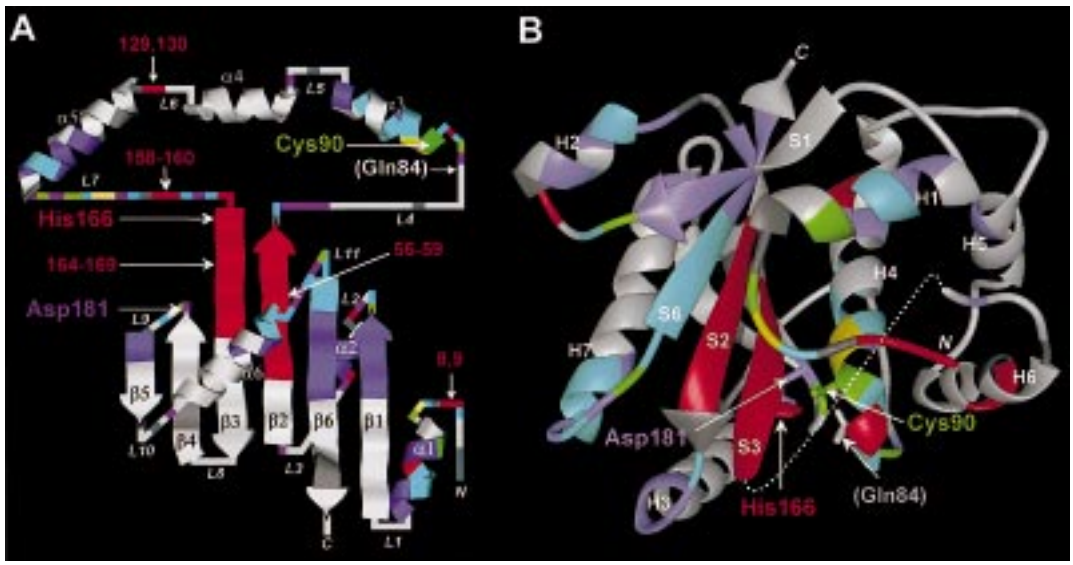

FIGURE 8: Chemical shift perturbation of backbone $^{1}H_N$, ^{15}N, and $^{13}C_\alpha$ nuclei in the YUH1−Ub covalent complex. (A) YUH1 residues affected by ubiquitin binding mapped onto the secondary structure of YUH1. (B) YUH1 residues affected by ubiquitin binding mapped onto the UCH-L3 crystal structure (*28*). The mean shift difference, Δ_{av}, for each amino acid was calculated as $[(\Delta^{1}H_N)^2 + (\Delta^{15}N)^2 + (\Delta^{13}C_\alpha)^2]^{1/2}$, where $\Delta^{1}H_N$, $\Delta^{15}N$, and $\Delta^{13}C_\alpha$ are the chemical shift differences (Hz) between free YUH1 and the YUH1−Ub complex for resonances $^{1}H_N$, ^{15}N, and $^{13}C_\alpha$ observed at 14.1 T (^{1}H frequency is 600 MHz), respectively. The rest of the representations and color coding are similar to those of Figure 6 except that the regions shown in red are those with conformational multiplicity (refer to text for details) in the YUH1−Ub complex.

not assigned, even though candidates existed with ^{1}H, ^{15}N, and intraresidue $^{13}C_\alpha$ correlations. For the well-resolved cross-peaks in ^{1}H−^{15}N HSQC but without sequential connectivities in triple-resonance experiments, where possible, tentative assignment of ^{1}H and ^{15}N resonances was done using the chemical shift values from the YUH1−Ub mixture (residues V8, T19, E41, Q71, and T134). Since YUH1 binds ubiquitin covalently in the complex (*9*), the low intensity in the triple-resonance experiments for these regions cannot be attributed to chemical exchange between the free and bound states. The most likely reason would be a local conformational multiplicity, which will be elaborated in the ensuing discussion.

Chemical Shift Mapping of the Ubiquitin Binding Interface. As mentioned earlier in the case of the YUH1−Ub mixture, the mean differences in ^{1}H, ^{15}N, and $^{13}C_\alpha$ chemical shifts of YUH1, Δ_{av}, for all backbone assigned residues in the YUH1−Ub complex were calculated. Figure 8 displays the chemical shift perturbation on the secondary structure of YUH1 and the tertiary structure of UCH-L3 in a representation similar to that of Figure 6 (^{1}H frequency was 600 MHz). To ensure clarity in interpretation, the residues lacking

perturbation data due to missing backbone assignment (~8% of non-proline residues) are shown in red and can be considered to exhibit conformational multiplicity. Consistent with our observations on the YUH1−Ub mixture, about 66% of the residues were unperturbed (Δ_{av} < 100 Hz) or showed negligible changes in chemical shifts (Δ_{av} < 200 Hz), indicating their distal location from the interaction surface. Interestingly, most of the residues (~20%) that were missing in the YUH1−Ub mixture displayed moderate to severe perturbations in the range of 200−2000 Hz. This supports our earlier assumption that disappearance of $^{1}H-^{15}N$ correlation cross-peaks in the YUH1−Ub mixture was due to extreme line broadening caused by the large chemical shift difference between ubiquitin bound and free states. As expected, some of the extremely perturbed residues were from regions lining the putative active site amino acids, originally identified by site-directed mutagenesis in UCH-L3 (*24*). Residues 86−92, 94, and 97 in helix α3 (helix H4 in UCH-L3) span the active site nucleophile C90 and are significantly perturbed ($\Delta_{av} \geq 500$ Hz) by ubiquitin binding. C90 shows a Δ_{av} of 632 Hz while G91 displayed the maximum Δ_{av} of 1330 Hz. Though D181, in loop L9 (between S4 and S5 in UCH-L3), a general acid for the catalysis, showed least perturbation, G182 displayed a Δ_{av} of 631 Hz, indicating that this region may still be functionally important. The X-ray structure of UCH-L3 (*28*) hinted at a role for Q84 in catalysis based on structural similarity with the catalytic center of papain family proteases. However, our results with the YUH1−Ub complex indicated only a weak perturbation for Q84 (86 Hz), though its importance cannot be completely ruled out. The large perturbation of residues, in the above-mentioned regions, suggests that extensive local conformational changes upon ubiquitin binding may be involved in stabilizing interactions around the active site of the enzyme.

Apart from these, residues with large chemical shift perturbation were also clustered in many other structured and loop regions. The N-terminal loop residues 7−13 constitute one such cluster that includes a highly conserved E12 residue. E12, the side chain of which was exposed in the UCH-L3 structure, showed a Δ_{av} of 1074 Hz and may contact the basic face of ubiquitin. The remaining residues displayed moderate perturbations (200 Hz ≤ Δ_{av} < 500 Hz). It can be seen from Figure 8B that this N-terminal loop partly covers the active site and so will have to be flexible to allow ubiquitin binding. Another stretch showing large-scale perturbation ($\Delta_{av} \geq 500$ Hz) upon ubiquitin binding is in loop L7 (disordered in UCH-L3), from residues 146 to 163, which was proposed to mask the active site (*28*). In this region, residues 158−160 lacked perturbation data, as they were unassigned in the complex. Residues 146, 149, 150, and 152−154 displayed severe perturbations ($\Delta_{av} \geq 500$ Hz), while residues 147, 148, 151, and 156 were moderately perturbed (200 Hz ≤ Δ_{av} < 500 Hz). This loop was thought to be involved in ubiquitin binding in UCH-L3 (*28*), and our experimental result with the YUH1−Ub complex confirms this possibility. I142, which displayed a large Δ_{av} in the YUH1−Ub mixture also showed a Δ_{av} of ~500 Hz in the YUH1−Ub complex, indicating probably a hydrophobic side-chain interaction with ubiquitin. Two other clusters, residues 215−218, partly in helix α6 and loop L11 (between H7 and S6 in UCH-L3), and residues 221−227 (S6 in UCH-L3), also displayed moderate perturbation (200 Hz ≤ Δ_{av} < 500 Hz), with V223 alone showing a Δ_{av} of 506 Hz. Thus these C-terminal regions may undergo a slight conformational change upon ubiquitin binding. It is noteworthy that most of the above-mentioned residues contributing to structural changes in YUH1 upon ubiquitin binding were line-broadened in the YUH1−Ub mixture.

A highly conserved hydrophobic cluster from residues 55 to 59 in β2 (S2 in UCH-L3) could not be assigned in the complex. Also for residues 164−169 in β3 (S3 in UCH-L3) spanning the general base in catalysis, H166, assignment was lacking in the complex. This region was predominantly hydrophobic. In addition to the above, V8 and V9 of the N-terminal loop, F129 and D130 of loop L6 (between H4 and H5) and residues 158−160 in loop L7 (disordered in UCH-L3) also lacked assignment. These regions were extremely broadened in the YUH1−Ub mixture. As stated before, with ubiquitin being stabilized in a covalent complex with YUH1, the possibility of chemical exchange between bound and free forms can be ruled out. We proposed a local conformational multiplicity to account for the line broadening in these regions. In fact, for residues in the loop region that surrounds the active site, a certain amount of flexibility can be imagined, essential to expose the active site to ubiquitin. A slight flexibility in these regions would also probably account for the hydrolysis of a wide range of extended ubiquitin C-terminal fusions ranging from simple amines to small proteins (a conserved feature in UCHs), as YUH1 lacked specificity for the leaving group. But for the strands β2 and β3 (S2 and S3 in UCH-L3), multiplicity is intriguing, as these are fairly rigid structures. Hence, alternate local conformation induced exchange broadening around the β-sheet regions is not a possibility anymore. However, if the loop regions interact with the above β-sheet regions through the side chains, then their flexibility might be propagated to strands β2 and β3, appearing as line broadening of backbone amide resonances. Strands β2 and β3 in YUH1 and in other UCH enzymes consist mostly of hydrophobic residues. In the crystal structure of UCH-L3, the side chains of these hydrophobic residues are exposed away from the protein core, with the N-terminal loop covering strand S2 (*28*). Also some contacts were found between the N-terminal loop residues and the β-sheet (*28*). Moreover, the flexible loop L7 (disordered in UCH-L3) can also interact with the β-sheet region through the hydrophobic residues. In addition to the above, the hydrophobic side chains of YUH1 could also interact with corresponding residues in ubiquitin, a possibility strongly supported by experiments that revealed many hydrophobic residues in the YUH1 binding surface of ubiquitin (Sakamoto et al., unpublished). Thus, the alternating orientations of side chains of hydrophobic residues in strands β2 and β3, resulting from intramolecular interactions with flexible loops (N-terminal and L7) or from intermolecular contacts with ubiquitin, may indirectly lead to large chemical shift differences for the backbone residues. This might appear as line broadening of backbone amide resonances in strands β2 and β3. The highly conserved nature of the above-mentioned hydrophobic residues among UCH enzymes probably indicates the importance of hydrophobic interactions and conformational multiplicity in ubiquitin recognition.

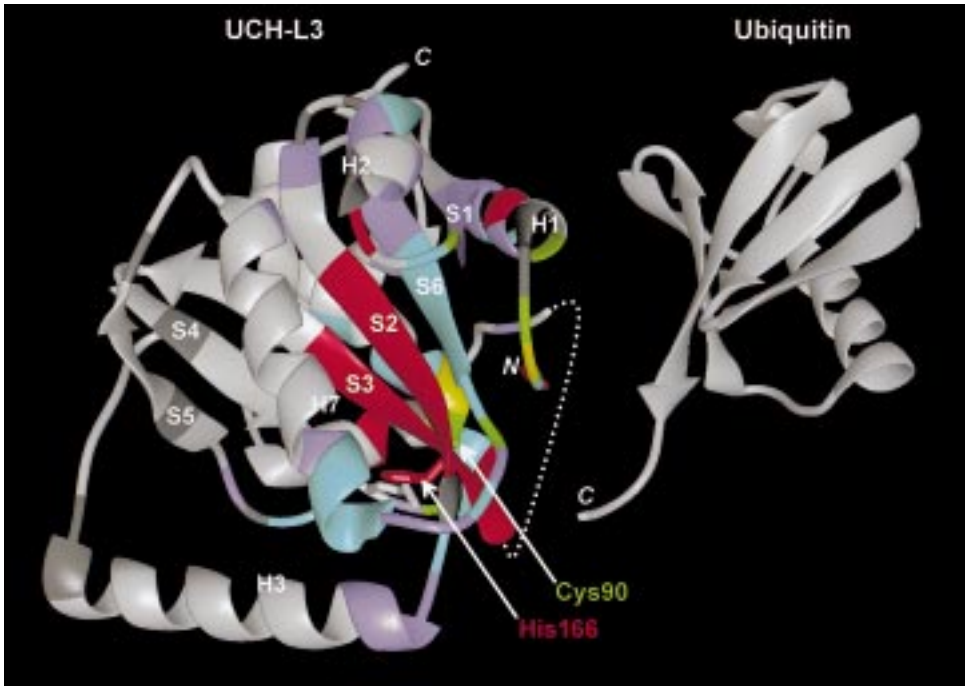

FIGURE 9: Proposed model for ubiquitin binding to UCH-L3 based on the ubiquitin binding surface mapping from the YUH1−Ub complex. This view of UCH-L3 is approximately perpendicular, from the left, to Figure 8B. The structure of ubiquitin (*49*) was oriented according to the mapping of the YUH1 binding interface on ubiquitin (Sakamoto et al., unpublished). The side chains of active site residues in UCH-L3 are highlighted.

YUH1−Ub Interaction Model. On the basis of the ubiquitin interacting surface delineated in this study, a hypothetical model for the YUH1− Ub complex could be envisaged by employing the crystal coordinates of UCH-L3 (*28*) and ubiquitin (*49*), as shown in Figure 9. The fact that most of the binding interface residues, outlined in our study, are conserved among UCH family members identified so far suggests that the ubiquitin recognition mechanism might also be conserved. The orientation of ubiquitin in this model was according to the YUH1 binding interface mapped onto the crystal structure of ubiquitin (Sakamoto et al., unpublished). In the UCH-L3 structure (*28*), the N-terminal loop and helix H4 were shown to occlude residues in the active site (the disordered loop too was proposed to mask the active site). To position the Gly76 carboxyl group of ubiquitin near the active site cysteine of UCH enzymes, these regions would have to undergo rearrangement. Our result, wherein strands β2, β3, and β6 (S2, S3, S6 in UCH-L3), helices α1 and α4 (H1 and H4 in UCH-L3), loop L7 (disordered loop in UCH-L3), and N-terminal residues of YUH1 undergo significant ubiquitin-induced conformational changes, confirms the above possibility. During this process there is also a possibility for ubiquitin structure proofreading, to limit the nonspecific hydrolysis by UCH enzymes. The crystal structure of free UCH-L3 did not reveal the presence of a deep narrow groove necessary to bind extended ubiquitin C-terminal fusions (*28*). Results from the YUH1−Ub complex indicate that such a deep substrate cleft of S1′ sites may be formed by the conformational changes occurring in response to ubiquitin binding. Recently, it was shown that UCH-L3 could cleave C-terminal extensions from a ubiquitin-like protein, NEDD8 (*51*). This and our studies reported here lend further support to the general perception that UCH enzymes recognize the overall structure of ubiquitin (or ubiquitin-like proteins) and undergo conformational changes necessary to cleave extended C-terminal fusions of ubiquitin.

Biochemical and thermodynamic studies on UCH-L3 indicated that UCH enzymes derive sufficient energy from remote interactions with ubiquitin to stabilize the acyl-enzyme reaction intermediate (*27*). Our NMR studies on YUH1 and the YUH1−Ub covalent complex, which mimics the transition-state analogue, prove that UCHs in general, and YUH1 in particular, undergo conformational changes upon binding to ubiquitin. These structural changes mediated by strong hydrophobic and ionic interactions between ubiquitin and enzyme provide the energy that stabilizes the transition-state intermediate, resulting in hydrolysis of substrates attached to the ubiquitin C-terminus. The results presented here provide the first detailed account of the ubiquitin binding sites for UCH enzymes using the YUH1−Ub complex as a model system. The function and importance of particular residues will now be further explored by site-directed mutagenesis.

ACKNOWLEDGMENT

We thank Drs. Ernest D. Laue, Daniel Nietlispach, and Brian O. Smith for numerous stimulating discussions. We are grateful to Dr. Judyth Sassoon for a critical reading of the manuscript and to Dr. Koji Takio for help in measurement on the DRX600 spectrometer at the Division of Biomolecular Characterization, RIKEN. S.R. thanks Prof. Nobuo Tsuchida of Tokyo Medical and Dental University for advice and guidance and the Ministry of Science, Education and Culture (Monbusho), Government of Japan, for financial support. Molecular graphics images were produced using the Midas-Plus software from the Computer Graphics Laboratory, University of California, San Francisco.

SUPPORTING INFORMATION AVAILABLE

Lists of backbone ^{1}H, ^{13}C, and ^{15}N resonance assignments for free YUH1, the YUH1−Ub mixture, and the YUH1−Ub covalent complex at 30 °C, pH 6.0. This material is available free of charge via the Internet at http://pubs.acs.org.

REFERENCES

1. Hochstrasser, M. (1996) *Annu. Rev. Genet. 30*, 405−439.
2. Pickart, C. M. (1997) *FASEB J. 11*, 1055−1066.
3. Varshavsky, A. (1997) *Trends Biochem. Sci. 22*, 383−387.
4. Hershko, A., and Ciechanover, A. (1998) *Annu. Rev. Biochem. 67*, 425−479.
5. Ozkaynak, E., Finley, D., Solomon, M. J., and Varshavsky, A. (1987) *EMBO J. 6*, 1429−1439.
6. Wilkinson, K. D. (1997) *FASEB J. 11*, 1245−1256.
7. Tobias, J. W., and Varshavsky, A. (1991) *J. Biol. Chem. 266*, 12021−12028.
8. Baker, R. T., Tobias, J. W., and Varshavsky, A. (1992) *J. Biol. Chem. 267*, 23364−23375.
9. Pickart, C. M., and Rose, I. A. (1986) *J. Biol. Chem. 261*, 10210−10217.
10. Papa, F. R., and Hochstrasser, M. (1993*) Nature 366*, 313−319.
11. Wilkinson, K. D., Tashayev, V. L., O'Connor, L. B., Larsen, C. N., Kasperek, E., and Pickart, C. M. (1995) *Biochemistry 34*, 14535−14546.
12. Huang, Y., Baker, R. T., and Fischer-Vize, J. A. (1995) *Science 270*, 1828−1831.
13. Gray, D. A., Inazawa, J., Gupta, K., Wong, A., Ueda, R., and Takahashi, T. (1995) *Oncogene 10*, 2179−2183.
14. Moazed, D., and Johnson, A. D. (1996) *Cell 86*, 667−677.
15. Zhu, Y., Carroll, M., Papa, F. R., Hochstrasser, M., and D'Andrea, A. D. (1996) *Proc. Natl. Acad. Sci. U.S.A. 93*, 3275−3279.
16. Zhu, Y., Lambert, K., Corless, C., Copeland, N. G., Gilbert, D. J., Jenkins, N. A., and D'Andrea, A. D. (1997) *J. Biol. Chem. 272*, 51−57.
17. Maki, A., Mohammad, R. M., Smith, M., and Al-Katib, A. (1996) *Differentiation 60*, 59−66.
18. Jensen, D. E., Proctor, M., Marquis, S. T., Gardner, H. P., Ha, S. I., Chodosh, L. A., Ishov, A. M., Tommerup, N., Vissing, H., Sekido, Y., Minna, J., Borodovsky, A., Schultz, D. C., Wilkinson, K. D., Maul, G. G., Barlev, N., Berger, S. L., Prendergast, G. C., and Rauscher, F. J. (1998) *Oncogene 16*, 1097−1112.
19. Liu, C.-C., Miller, H. I., Kohr, W. J., Jr, and Silber, J. I. (1989) *J. Biol. Chem. 264*, 20331−20338.
20. Wilkinson, K. D., Lee, K., Deshpande, S., Duerksen-Hughes, P., Boss, J. M., and Pohl, J. (1989) *Science 246*, 670−673.
21. Zhang, N., Wilkinson, K. D., and Bownes, M. (1993) *Dev. Biol. 157*, 214−223.
22. Larsen, C. N., Price, J. S., and Wilkinson, K. D. (1996) *Biochemistry 35*, 6735−6744.
23. Miller, H. I., Henzel, W. J., Ridgeway, J. B., Kuang, W., Chisholm, V., and Liu, C.-C. (1989) *Biotechnology 7*, 698−704.
24. Larsen, C. N., Krantz, B. A., and Wilkinson, K. D. (1998) *Biochemistry 37*, 3358−3368.
25. Schechter, I., and Berger, A. (1967) *Biochem. Biophys. Res. Commun. 27*, 157−162.
26. Fox, T., Mason, P., Storer, A., and Mort, J. S. (1995) *Protein Eng. 8*, 53−57.
27. Dang, L. C., Melandri, F. D., and Stein, L. R. (1998) *Biochemistry 37*, 1868−1879.
28. Johnston, S. C., Larsen, C. N., Cook, W. J., Wilkinson, K. D., and Hill, C. P. (1997) *EMBO J. 16*, 3787−3796.
29. Kohno, T., Kusunoki, H., Sato, K., and Wakamatsu, K. (1998) *J. Biomol. NMR 12*, 109−121.
30. Sambrook, J., Fritsch, E. F., and Maniatis, T. (1989) in *Molecular Cloning: A Laboratory Manual*, Cold Spring Harbor Press, Cold Spring Harbor, NY.
31. Laue, E. D., Mayger, M. R., Skilling, J., and Staunton, J. (1986) *J. Magn. Reson. 68*, 14−29.
32. Kraulis, P. J. (1989) *J. Magn. Reson. 84*, 627−633.
33. Kraulis, P. J., Domaille, P. J., Campbell-Burk, S. L., Van Aken, T., and Laue, E. D. (1994) *Biochemistry 33*, 3515−3531.
34. Ikura, M., Kay, L. E., and Bax, A. (1990) *Biochemistry 29*, 4659−4667.
35. Grzesiek, S., and Bax, A. (1992) *J. Magn. Reson. 96*, 432−440.
36. Yamazaki, T., Lee, W., Revington, M., Mattiello, D. L., Dahlquist, F. W., Arrowsmith, C. H., and Kay, L. E. (1994) *J. Am. Chem. Soc. 116*, 6464−6465.
37. Bax, A., and Ikura, M. (1991) *J. Biomol. NMR 1*, 99−104.
38. Yamazaki, T., Lee, W., Arrowsmith, C. H., Muhandiram, D. R., and Kay, L. E. (1994) *J. Am. Chem. Soc. 116*, 11655−11666.
39. Grzesiek, S., and Bax, A. (1992) *J. Am. Chem. Soc. 114*, 6291−6293.
40. Nietlispach, D., Clowes, R. T., Broadhurst, R. W., Ito, Y., Keeler, J., Kelly, M., Ashurst, J., Oschkinat, H., Domaille, P. J., and Laue, E. D. (1996) *J. Am. Chem. Soc. 118*, 407−415.
41. Grzesiek, S., Anglister, J., Ren, H., and Bax, A. (1993) *J. Am. Chem. Soc. 115*, 4369−4370.
42. Boucher, W., Laue, E. D., Campbell-Burk, S., and Domaille, P. J. (1992) *J. Am. Chem. Soc. 114*, 2262−2264.
43. Wishart, D. S., and Sykes, B. D. (1994) *J. Biol. NMR 4*, 171−180.
44. Wishart, D. S., and Sykes, B. D. (1991) *J. Mol. Biol. 222*, 311−333.
45. Wuthrich, K. (1986) in *NMR of Proteins and Nucleic Acids*, John Wiley and Sons, NewYork.
46. Farmer, B. T., II, and Venters, R. A. (1995) *J. Am. Chem. Soc. 117*, 4187−4188.
47. Venters, R. A., Metzler, W. J., Spicer, L. D., Mueller, L., and Farmer, B. T., II (1995) *J. Am. Chem. Soc. 117*, 9592−9593.
48. Grzesiek, S., Wingfield, P., Stahl, S., Kaufman, J. D., and Bax, A. (1995) *J. Am. Chem. Soc. 117*, 9594−9595.
49. Vijay-Kumar, S., Bugg, C. E., and Cook, W. J. (1987) *J. Mol. Biol. 194*, 531−544.
50. Vijay-Kumar, S., Bugg, C. E., and Cook, W. J. (1987) *J. Biol. Chem. 262*, 6396−6399.
51. Wada, H., Kito, K., Caskey, L. S., Yeh, E. T. H., and Kamitani, K. (1998) *Biochem. Biophys. Res. Commun. 251*, 688−692.
52. Rost. B., and Sander, C. (1993) *Proc. Natl. Acad. Sci. U.S.A. 90*, 7558−7562.

BI9903953